
Automatic Discovery of One Parameter Subgroups of $SO(n)$

Pavan Karjol

Indian Institute of Science
Bengaluru, Karnataka

Vivek V Kashyap

Indian Institute of Science
Bengaluru, Karnataka

Rohan Kashyap

Carnegie Mellon University
Pittsburgh, Pennsylvania, USA

Prathosh A P

Indian Institute of Science
Bengaluru, Karnataka

Abstract

We introduce a novel framework for the automatic discovery of one-parameter subgroups (H_γ) of $SO(3)$ and, more generally, $SO(n)$. One-parameter subgroups of $SO(n)$ are crucial in a wide range of applications, including robotics, quantum mechanics, and molecular structure analysis. Our method utilizes the standard Jordan form of skew-symmetric matrices, which define the Lie algebra of $SO(n)$, to establish a canonical form for orbits under the action of H_γ . This canonical form is then employed to derive a standardized representation for H_γ -invariant functions. By learning the appropriate parameters, the framework uncovers the underlying one-parameter subgroup H_γ . The effectiveness of the proposed approach is demonstrated through tasks such as double pendulum modeling, moment of inertia prediction, top quark tagging and invariant polynomial regression, where it successfully recovers meaningful subgroup structure and produces interpretable, symmetry-aware representations. Our implementation is available here¹.

1 Introduction

Invariance and equivariance are fundamental principles in neural network design, providing crucial inductive biases that enhance performance and generalization. This has led to the development of Group-equivariant Convolutional Neural Networks (G-CNNs), which extend the translational equivariance of standard CNNs to more general group actions like rotations and reflections [1]. This innovation spurred significant progress in the field, including harmonic networks tailored for rotational equivariance [2], tensor field networks designed for 3D geometric data [3], $SE(3)$ -transformers for modeling molecular and physical systems [4], and steerable 3D CNNs [5]. Furthermore, the Deep Sets framework [6] introduced permutation-invariant learning, and Steerable CNNs [7] broadened the scope of equivariant modeling to continuous groups.

In many real-world scenarios, the underlying symmetries of a task are unknown. Uncovering these hidden symmetries is crucial for effectively learning the underlying function from observed data. A promising approach towards this goal lies in the automatic discovery of one-parameter subgroups within Lie groups, with a specific focus on the Special Orthogonal group $SO(n)$. Importantly, one-parameter subgroups also provide insight into higher-dimensional Lie subgroups, making their automated discovery a valuable tool for symmetry-aware learning in scientific computing and beyond. The group $SO(n)$ is central to modeling rotational symmetries in n dimensions, a ubiquitous aspect of many physical systems. A one-parameter subgroup, formally defined as the image of a Lie group homomorphism [8], serves as a fundamental building block for understanding more

¹https://anonymous.4open.science/r/Automatic_discovery_so_n-7664/

complex Lie group symmetries [9]. Notably, in the context of 3D rotations ($SO(3)$), all non-trivial connected subgroups are one-parameter subgroups [10], underscoring their importance in capturing rotational invariance. In this work, we direct our attention towards the discovery of such one-parameter subgroups, referring to the image of a homomorphism γ that generates such a subgroup as H_γ . These types of symmetry groups are not merely theoretical constructs; they arise naturally in various applications. For instance, in quantum mechanics, the Hamiltonian of the hydrogen atom exhibits $SO(3)$ invariance. The non-commutative nature of 3D rotations leads to the organization of eigenfunctions according to the irreducible representations of $SO(3)$, characterized by angular momentum quantum numbers. This structure allows for the simplification of the eigenvalue problem to a one-dimensional form through the separation of variables in spherical harmonics.

Beyond physics, discovering one-parameter subgroups is critical in robotics [11], molecular modeling [12], double pendulum system modeling [13] and computer vision [14], where rotational symmetries underpin model behavior and interpretation. In $SO(3)$, these subgroups correspond to identifying rotation axes, while in higher dimensions they encode more complex symmetries.

In this work, we introduce a practical framework for learning one-parameter subgroups H_γ of $SO(n)$ and constructing invariant functions. Our method is computationally efficient, requires no symmetry supervision, and naturally integrates symmetry discovery with learning. This advances symmetry-based modeling by enabling neural networks to discover and leverage structure directly from data.

1.1 Contributions

- We introduce a canonical form for any H_γ -invariant function, where H_γ represents a one-parameter subgroup of $SO(3)$. Leveraging this standard form, we develop a method for automatic symmetry discovery in one-parameter subgroups of $SO(3)$.
- We analyze the orbit structure under one-parameter subgroup (H_γ) of $SO(n)$ and provide a standard representation element for any such orbit. This representation fully characterizes the orbits under the action of H_γ .
- Extending our results from $SO(3)$, we utilize the standard representation element of orbit structure to propose a canonical form for any H_γ -invariant function in the case of $SO(n)$. This formulation enables automatic symmetry discovery for one-parameter subgroups of $SO(n)$.
- We evaluate our framework across diverse tasks, including invariant polynomial regression, symmetry modeling in anisotropic quantum systems, double pendulum system modeling, moment of inertia prediction, and Top quark tagging—demonstrating broad applicability in both synthetic and real-world settings.

2 Related work

2.1 Group Equivariance

In recent years, the application of symmetries in deep learning has attracted considerable attention within the research community [15]. A notable contribution in this direction was made by [1], who introduced G -equivariant neural networks as a principled generalization of Convolutional Neural Networks (CNNs) to incorporate a broader class of symmetries beyond translations. This foundational work was extended by [16], who formalized convolution operations under arbitrary compact groups, and further developed by [17] through the application of equivariant linear maps on homogeneous spaces. Complementarily, data augmentation techniques have played a key role in implicitly instilling invariance into models, allowing them to learn robustness to specific transformations [18–20].

Building on these theoretical advancements, several practical models have been proposed to realize group equivariance across different data modalities. Equivariant Graph Neural Networks [21] are designed to preserve equivariance to Euclidean transformations in 3D space, which is particularly relevant for molecular and physical systems. [22] introduced 3D Steerable CNNs, which construct rotation-equivariant features in volumetric data using steerable filter bases. This idea was further generalized in [23] through learning steerable filters capable of handling continuous rotation groups. Meanwhile, [24] proposed Geometric Clifford Algebra Networks, leveraging the expressiveness of

Clifford algebras to model orthogonal group invariances. Lastly, G-RepsNet by [25] offers a fast and general construction for building equivariant neural networks under arbitrary matrix groups, broadening the applicability of equivariant methods.

2.2 Lie Groups

[26] extracts group symmetries directly in the form of corresponding Lie group generator using a polarization matrix. LieConv [27] construct a convolutional layer that is equivariant to transformations from any specified Lie group with a surjective exponential map. A more common approach is to discretize the group [5, 22, 1] or use a truncated sum over irreducible representations [7] using spherical harmonics [2]. [28] utilize the Clebsch-Gordon decomposition for $SO(3)$ -equivariant neural network architecture for spherical data that operates completely in Fourier space. [13] propose a general method for constructing equivariant multilayer perceptrons (MLPs) for arbitrary matrix groups, thereby extending the applicability of equivariant deep learning models beyond commonly studied groups like $SO(n)$ and $O(n)$. An automatic Lie group symmetry discovery method is proposed, employing Lie algebra convolutions [29]. Unlike our approach, which operates on vectors, this method employs Lie algebra convolutions on feature maps, resulting in a different group action.

[30] utilize the lie derivative to evaluate the degree to which a function violates a symmetry. While their methodology focuses on evaluating equivariance in pre-trained models, our approach fundamentally differs by incorporating symmetry principles intrinsically into the neural network architecture through principled design choices and structural constraints, ensuring equivariance by construction.

2.3 Automatic Symmetry Discovery

There is growing interest in automatically discovering symmetries from data, particularly in settings where the symmetry group is unknown. Broadly, methods vary in whether they (i) discover symmetries jointly during training or post hoc, (ii) learn equivariant models directly, and (iii) incorporate structural inductive biases for sample efficiency and interpretability.

LieGG [26] identifies Lie group symmetries by analyzing the behavior of a trained, unconstrained network. While general, it does not produce an equivariant model and lacks the sample efficiency benefits of built-in inductive biases. LieGAN [31] discovers generators of Lie algebras through adversarial learning, but a separate architecture must be manually constructed using the discovered symmetry for downstream tasks. Augerino [32] learns a distribution over transformations and averages predictions over transformed inputs to approximate invariance. While this avoids the need for explicit symmetry encoding, the predictor network remains unstructured and not inherently equivariant, resulting in reduced interpretability and increased test-time cost due to averaging of predictions over multiple transformed inputs. Bispectral Neural Networks (BNNs) [33] construct equivariant models using bispectral features derived from harmonic analysis. However, they rely on finite approximations despite offering strong inductive biases.

In contrast, our method jointly discovers one-parameter subgroups of $SO(n)$ and learns the underlying function within an end-to-end framework, yielding interpretable symmetry-aware models.

3 Background

Definition 3.1. A **group** (G, \cdot) is a set G with a binary operation $\cdot : G \times G \rightarrow G$ satisfying associativity, identity, and inverse properties.

Definition 3.2. A **subgroup** (H, \cdot) of a group G is a subset $H \subseteq G$ that forms a group under the group operation of G .

Definition 3.3. A **group action** of a group G on a set X is a function $\phi : G \times X \rightarrow X$ satisfying: $\phi(e, x) = x, \forall x \in X$, and $\phi(g, \phi(h, x)) = \phi(gh, x), \forall g, h \in G, x \in X$.

Definition 3.4. The **orbit** of an element $x \in X$ under a group action ϕ is the set $\text{Orb}(x) = \{\phi(g, x) \mid g \in G\}$.

Definition 3.5. A **homomorphism** between two groups G and H is a function $\varphi : G \rightarrow H$ satisfying $\varphi(g_1g_2) = \varphi(g_1)\varphi(g_2)$ for all $g_1, g_2 \in G$.

Definition 3.6. The **special orthogonal group** $SO(n)$ is the group of $n \times n$ real matrices R satisfying $R^T R = I$ and $\det(R) = 1$.

Definition 3.7. A **2D rotation matrix** is a 2×2 matrix of the form $R(t) = \begin{bmatrix} \cos t & -\sin t \\ \sin t & \cos t \end{bmatrix}$.

Definition 3.8. A **3D rotation matrix about the z -axis** is given by, $R_z(t) = \begin{bmatrix} R(t) & \mathbf{0} \\ \mathbf{0}^T & 1 \end{bmatrix}$, where $R(t)$ is the 2D rotation matrix as defined in 3.7.

4 Proposed method

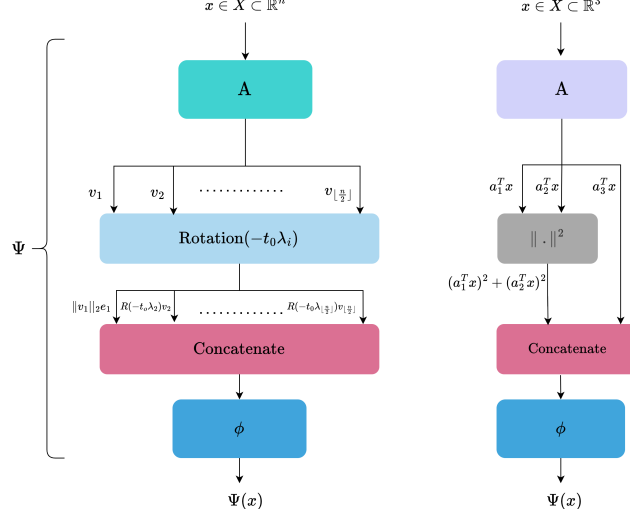


Figure 1: Block diagram of the proposed H_γ^{inv} -Net framework for discovering one-parameter subgroups of $SO(n)$ (left) and $SO(3)$ (right). The framework learns a rotation matrix A and rotation rates λ to construct a canonical invariant representation. Theorems 4.6 and 4.2 provide the theoretical basis for expressing any H_γ -invariant function in a standard form, facilitating the discovery of underlying one-parameter subgroups for $SO(n)$ and $SO(3)$. The model is trained end-to-end using gradient descent on $x \in [0, 1]^n$ (n is even for $SO(n)$ case).

We address the problem of learning an H_γ -invariant function $f : X \rightarrow \mathbb{R}^m$, where $X = [0, 1]^n \in \mathbb{R}^n$ and H_γ is a one-parameter subgroup of $SO(n)$ that is unknown. The function f must satisfy the invariance condition: $f(h \cdot x) = f(x)$, $\forall h \in H_\gamma$ and $x \in X$, where $h \cdot x$ denotes the group action of h on x . Our primary goal is to automatically discover the underlying symmetry subgroup H_γ directly from the given data samples while simultaneously learning the invariant function f . This framework enables effective learning of H_γ -invariant functions in scenarios where the symmetry is not explicitly provided, with potential applications in areas such as physical simulations, molecular modeling, and dynamical systems where underlying symmetries might be present but are not readily apparent.

4.1 Learning H_γ -invariant Functions: $SO(3)$

We leverage the norm-invariance property of rotational symmetry to derive a standard form for H_γ -invariant functions, where H_γ is a one-parameter subgroup of $SO(3)$.

Remark 4.1. Any one-parameter subgroup of $SO(3)$ is isomorphic to $SO(2)$. For an arbitrary axis defined by a rotation matrix $A \in SO(3)$, the one-parameter subgroup is given by:

$$H := \{A^T R_z(t) A : t \in \mathbb{R}\}, \quad (1)$$

where $R_z(t)$ is as defined in 3.8.

To formalize this idea, we present the following theorem:

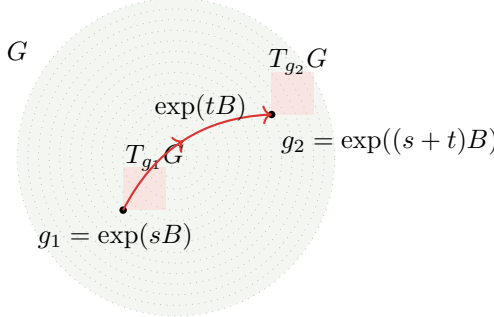


Figure 2: Visualization of one-parameter subgroups on Lie group G through the exponential map.

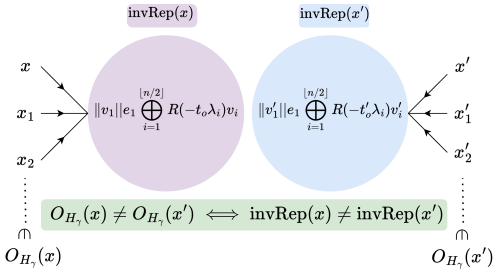


Figure 3: Visualization of the invariant representation (invRep) and its relationship to the orbits of H_γ . Each orbit $\mathcal{O}_{H_\gamma}(x)$ is mapped to a unique invariant representation $\text{invRep}(x)$, ensuring a bijective correspondence.

Theorem 4.2 (One-parameter subgroups of $SO(3)$). *Any H_γ -invariant function of the form $\Psi : X \subseteq \mathbb{R}^3 \rightarrow \mathbb{R}^m$ can be expressed as:*

$$\Psi(x) = \phi \left(\left(a_1^T x \right)^2 + \left(a_2^T x \right)^2, a_3^T x \right), \quad (2)$$

for some $\phi : \mathbb{R}^2 \rightarrow \mathbb{R}^m$, where $\{a_i^T\}$ are rows of some $A \in SO(3)$.

The Appendix contains detailed proofs of all the theoretical results.

We utilize the standard form of H_γ -invariant functions to develop a novel framework for learning H_γ -invariant functions from data samples.

4.2 Joint Discovery of H_γ and Learning Invariant Functions

Given a dataset $\{(x_i, y_i = f(x_i))\}_{i \in [m]}$ where f is invariant under an unknown one-parameter subgroup H_γ of $SO(3)$, our goal is to jointly discover H_γ and learn f . We implement the function ϕ in equation 2 using a neural network, reusing the symbol ϕ for simplicity. The discovery and learning process jointly optimizes the rotation matrix $A \in SO(3)$ and the network weights θ by solving:

$$\arg \min_{\theta, A} \sum_{i=1}^m \mathcal{L} \left(y_i, \phi \left(\left(a_1^T x_i \right)^2 + \left(a_2^T x_i \right)^2, a_3^T x_i \right) \right), \quad (3)$$

where the learned matrix A defines the one-parameter subgroup H_γ as described in equation 1. Note that A and $AR_z(t)$ correspond to the same H_γ , and f might be invariant with respect to the entire $SO(3)$ group, leading to potential variations in the learned A compared to A_0 . This behavior is further elaborated in section 6 (Results and Discussion) and the Appendix.

We now extend the result of Theorem 4.2 to $SO(n)$ by first reviewing the Lie algebra of $SO(n)$ and its relation to one-parameter subgroups.

4.3 One-Parameter Subgroups

The Lie algebra $\mathfrak{g} = T_I G$ is the tangent space at the identity of a Lie group G . Each $B \in \mathfrak{g}$ defines a one-parameter subgroup via the homomorphism $\gamma : \mathbb{R} \rightarrow G$ with $\gamma(0) = I$, $\gamma'(0) = B$. The exponential map $\exp(B) = \sum_{k=0}^{\infty} \frac{B^k}{k!}$ maps \mathfrak{g} to G and satisfies $\gamma(t) = \exp(tB)$ [8], yielding the one-dimensional Lie subgroup:

$$H_\gamma = \{\exp(tB) \mid t \in \mathbb{R}\} = \text{Img}(\gamma). \quad (4)$$

This concept of one-parameter subgroups is visually illustrated in Fig. 2.

For $G = SO(n)$, the Lie algebra $\mathfrak{so}(n) = \{B \in \mathbb{R}^{n \times n} \mid B = -B^T\}$ consists of skew-symmetric matrices. Any $B \in \mathfrak{so}(n)$ admits the canonical block decomposition [10]:

$$B \sim \bigoplus_{k=1}^{\lfloor n/2 \rfloor} \begin{pmatrix} 0 & \lambda_k \\ -\lambda_k & 0 \end{pmatrix} \oplus (0)_{n \bmod 2},$$

where $\lambda_k \geq 0$ denote rotation rates in orthogonal 2D planes.

Applying the exponential yields a block-diagonal rotation:

$$\exp(tB) = A^T \left(\bigoplus_{k=1}^{\lfloor n/2 \rfloor} R(t\lambda_k) \oplus I_{n \bmod 2} \right) A,$$

where $R(t\lambda_k)$ is the 2D rotation matrix from Definition 3.7, and $A \in SO(n)$ specifies the orientation. Substituting into equation 4, the resulting one-parameter subgroup is given by:

$$H_\gamma = \left\{ A^T \left(\bigoplus_{k=1}^{\lfloor n/2 \rfloor} R(t\lambda_k) \oplus I_{n \bmod 2} \right) A \mid t \in \mathbb{R} \right\}. \quad (5)$$

Thus, discovering a one-parameter subgroup of $SO(n)$ reduces to learning the rotation rates $\{\lambda_k\}_{k=1}^{\lfloor n/2 \rfloor}$ and the invariant planes' orientation defined by A .

4.4 Learning H_γ -invariant functions: $SO(n)$

We now apply the Lie algebraic framework introduced in the previous section to characterize a canonical form for H_γ -invariant functions. The following construction defines an invariant representation under the action of a one-parameter subgroup H_γ , which will be used to derive a standard form for H_γ -invariant functions. We assume n is even.

Definition 4.3 (Invariant representation: `invRep`). Let $x \in \mathbb{R}^n$, $A \in SO(n)$, and $\{\lambda_i\}_{i=1}^{n/2}$ be rotation rates. Define $v = Ax$ and decompose $v = \bigoplus_{i=1}^{n/2} v_i$, where each $v_i \in \mathbb{R}^2$. Let $e_1 = [1, 0]^T$. Then the invariant representation is:

$$\text{invRep}\left(x; A, \{\lambda_i\}_{i \in [n/2]}\right) := \|v_1\|_2 e_1 \bigoplus_{i=2}^{n/2} R(-t_0 \lambda_i) v_i,$$

where t_0 satisfies $R(t_0 \lambda_1) e_1 = v_1 / \|v_1\|_2$, and $R(\cdot)$ denotes the standard 2×2 rotation matrix.

For notational simplicity, we omit A and $\{\lambda_i\}$ from the arguments of `invRep`.

With the function `invRep` defined, we now establish its connection to the orbit structure under the action of H_γ . The following proposition shows that each orbit can be represented using a transformed version of `invRep`(x).

Proposition 4.4 (Orbit Representation). Let H_γ be a one-parameter subgroup of $SO(n)$ defined by $A \in SO(n)$ and rotation rates $\{\lambda_i\}$. For any $x \in \mathbb{R}^n$, its orbit under the action of H_γ is

$$\mathcal{O}_{H_\gamma}(x) = \mathcal{O}_{H_\gamma}(A^T \text{invRep}(x)).$$

The above proposition establishes that the orbit of any point x can be expressed in terms of `invRep`(x). Next, we formalize the fact that `invRep` provides a complete characterization of these orbits, meaning that two points belong to the same orbit if and only if they have the same `invRep` representation.

Proposition 4.5 (Orbit Separation). The function `invRep` is in bijective correspondence with the orbits of X under the action of the one-parameter subgroup H_γ . Specifically, for any $x, x' \in \mathbb{R}^n$,

$$\mathcal{O}_{H_\gamma}(x) = \mathcal{O}_{H_\gamma}(x') \iff \text{invRep}(x) = \text{invRep}(x').$$

Hence, `invRep` is both invariant under H_γ and separates the orbits of H_γ .

Table 5.1: Comparison of H_γ^{inv} -Net (ours), LieGAN [31], and Augerino [32] on various H_γ -invariant polynomial tasks. For each method, we report the mean value of the relevant metric, with standard deviations provided in the Appendix. A dash (–) indicates a metric not applicable to that method. The bolded values represent the best (lowest) performance for each metric within a task.

Task	Method	Invariance Error	Val. Loss (MSE)	Cosine distance
$p(x)$ $n = 3$	H_γ^{inv} -Net	1.98×10^{-5}	2.46×10^{-6}	1.62×10^{-2}
	LieGAN	8.21×10^{-4}	–	–
	Augerino	1.27×10^{-3}	1.22×10^{-2}	–
$q(x)$ $n = 4$	H_γ^{inv} -Net	3.00×10^{-4}	5.94×10^{-2}	4.03×10^{-6}
	LieGAN	5.63×10^{-2}	–	–
	Augerino	2.12×10^{-2}	1.20×10^{-1}	–
$r(x)$ $n = 8$	H_γ^{inv} -Net	5.83×10^{-2}	4.78×10^{-1}	6.63×10^{-3}
	LieGAN	4.89×10^1	–	–
	Augerino	0.21×10^1	0.19×10^1	–

This result is illustrated in Fig. 3. Since invRep completely characterizes the orbits under the action of H_γ , it can be used to define a canonical form for H_γ -invariant functions, as stated below:

Theorem 4.6 (One-parameter subgroups of $SO(n)$). *Any H_γ -invariant function of the form $\Psi : X \subseteq \mathbb{R}^n \rightarrow \mathbb{R}^m$ can be expressed as*

$$\Psi(x) = \phi \left(\text{invRep} \left(x; A, \{\lambda_i\}_{i \in [n/2]} \right) \right), \quad (6)$$

for some function $\phi : \mathbb{R}^n \rightarrow \mathbb{R}^m$, where $A \in SO(n)$ and $\{\lambda_i\}$ are the rotation rates.

The case where n is odd requires minor modifications to the definition of the function invRep which are detailed in the Appendix. The subsequent results remain unchanged.

Similar to the $SO(3)$ case presented in equation 3, we leverage Theorem 4.6 to learn H_γ -invariant functions by jointly optimizing the network parameters θ , the matrix A , and the rotation rates λ . The overall method is illustrated in Fig. 1.

5 Experiments

We assess the performance of **our method, denoted as H_γ^{inv} -Net**, on both synthetic and real-world tasks involving functions invariant to one-parameter subgroups. The objective is to assess the framework’s ability to jointly discover the underlying symmetry H_γ and learn functions that are invariant to these discovered subgroups. We compare our method against EMLP [13] (which assumes known symmetries), as well as symmetry discovery methods such as LieGAN [31] and Augerino [32].

5.1 Synthetic Tasks: Learning H_γ -Invariant Polynomials

We evaluate H_γ^{inv} -Net on polynomial regression tasks where the target functions are invariant under an unknown one-parameter subgroup H_γ of $SO(3)$ or $SO(n)$. These symmetries are not provided to the model and must be discovered from data during training. Each polynomial defines a distinct H_γ -invariant function determined by its associated subgroup structure. The definitions of these polynomials are provided in the Appendix due to space constraints.

5.2 Real-World Symmetry Discovery

We test our method on real-world or physically motivated tasks, detailed below.

Anisotropic Quantum System: We consider the H_γ -invariant function $f(x) = \sum_{i=1}^{n/2} w_i((A_0 x)_{2i-1}^2 + (A_0 x)_{2i}^2)$, arising from a quantum system with an anisotropic Hamiltonian H , where $A_0 \in SO(n)$ defines preferred spatial axes and w_i are characteristic parameters.

The task is to learn both A_0 and the function f , given the data samples $\{(x_i, f(x_i))\}_i$.

Double Pendulum with Spring Coupling: This task involves predicting the spring force $f = \pm k(q_1 - q_2)$ from the positions and momenta of two pendulums, where q_1 and q_2 denote the angles of the pendulums with respect to the z -axis. The underlying symmetry of this system is $SO(2) \oplus SO(2)$, characterized by rotation rates $[1, 1, 0]$, with the 0 indicating no invariance in the momenta.

Moment of Inertia Prediction: We predict the inertia matrix given by $\sum_{i=1}^N m_i(x_i^T x_i I - x_i x_i^T)$ from masses and positions of N points. This function is equivariant under the group $\bigoplus_{i=1}^N SO(3)$, and consequently, also equivariant under its one-parameter subgroups $\cong \bigoplus_{i=1}^N SO(2)$. Our method successfully identifies one of these subgroups and learns the corresponding equivariant function. The extension of H_γ^{inv} -Net to handle equivariance is straightforward and detailed in the Appendix.

Table 5.2: Comparison of invariance error, validation loss, and cosine distance across different methods on three H_γ -invariant tasks. A dash (–) indicates a metric not applicable to that method. The bolded values represent the best (lowest) performance for each metric within a task.

Task	Method	Invariance Error	Val. Loss (MSE)	Cosine distance
Anisotropic Quantum $n = 4$	H_γ^{inv} -Net	7.92×10^{-2}	1.21×10^{-6}	2.72×10^{-3}
	EMLP	–	2.90×10^{-2}	–
	LieGAN	1.15×10^{-1}	–	–
Double Pendulum $n = 8$	H_γ^{inv} -Net	1.7×10^{-1}	5.59×10^{-6}	4.76×10^{-5}
	EMLP	–	1.53×10^{-6}	–
	LieGAN	4.10×10^{-1}	–	–
Moment of Inertia $n = 3$	H_γ^{inv} -Net	1.90×10^{-5}	3.00×10^{-6}	4.4×10^{-9}
	EMLP	–	1.36×10^{-3}	–
	LieGAN	3.09×10^{-4}	–	1.91×10^{-6}
	Augerino	2.60×10^0	6.03×10^{-3}	1.95×10^{-1}

6 Results and Discussion

We evaluate each method using the following metrics: (i) **Validation loss**, which measures prediction accuracy on held-out data; (ii) **Cosine distance**, which quantifies alignment between the learned and reference Lie algebra generators; and (iii) **Invariance error** (similar to the ‘symmetry variance’ criterion proposed by [26]), given by $\mathbb{E}_{h, x} [\mathcal{L}(f(x), f(h \cdot x))]$, which evaluates how well the learned invariance captures the underlying symmetry of the function. We estimate this over random samples of h from the discovered subgroup and x from the unit hypercube.

For H_γ^{inv} -Net, the learned parameters A and λ are directly interpretable and comparable to known ground truths, enabling us to report cosine distances for all tasks. In contrast, LieGAN and Augerino lack this explicit interpretability; thus, comparing their learned symmetries to known candidate ground truths can yield high cosine distances, particularly when these methods correctly discover alternative valid symmetries we have not explicitly identified. To fairly evaluate all methods irrespective of this mismatch, we also report invariance error for all the methods.

6.1 Quantitative Comparison

H_γ^{inv} -Net consistently achieves lower validation losses and invariance errors across all synthetic and real-world tasks considered (see Tables 5.1 and 5.2). Additionally, it attains cosine distances near zero, indicating close alignment with the reference Lie algebra generators.

Although LieGAN and Augerino show competitive results in some cases (e.g., LieGAN in moment of inertia prediction task and Augerino in low-dimensional settings), H_γ^{inv} -Net consistently outperforms both methods across all metrics. Unlike LieGAN, which solely performs symmetry discovery, H_γ^{inv} -Net jointly discovers symmetries and learns the corresponding invariant function. Furthermore,

Augerino exhibits instability in higher dimensions, whereas H_γ^{inv} -Net remains robust. Additionally, H_γ^{inv} -Net accurately recovers the rotation rates λ , as shown in Table 6.1.

EMLP is provided with the exact symmetry and serves as an oracle baseline. In the double pendulum task, although EMLP achieves lower validation loss, our method—which discovers the symmetry from data without prior knowledge—outperforms all other symmetry discovery approaches.

Table 6.2 highlights the conceptual advantages of our method over existing approaches—particularly in combining strong inductive bias, interpretability within a unified (end-to-end) framework.

Table 6.1: Comparison of reference rotation rates λ_0 and those learned by H_γ^{inv} -Net(our method) across tasks. Since rates are relative, the first value is fixed to 1. The model accurately recovers the underlying rotation rates, demonstrating effective symmetry discovery across various tasks.

Task	λ_0 (Reference)	λ (Learned)
$q(x)$	1, 1	1, 0.9999
$r(x)$	1, 1, 1, 1	1, 0.9998, 0.9992, 1.0002
Anisotropic Quantum System	1, 1	1, 0.99
Double Pendulum	1, 1, 0	1, 0.9889, 0.0007
Top Quark Tagging	1, 0	1, 0.00008

6.2 Interpretability

We observe that the learned rotation matrix A typically aligns with a transformed version of the ground truth A_0 . For example, in the $SO(3)$ case, the relationship can be expressed as $A \approx A_0 R_z(t)$, where $R_z(t)$ is as defined in Definition 3.8. Thus, A corresponds to the same one-parameter subgroup as A_0 . In higher-dimensional $SO(n)$ settings, the relation is more intricate; however, we provide a theoretical result in the Appendix that specifies conditions under which $A_0^T A$ implies equivalence of the underlying subgroups. These conditions hold consistently in our experiments (see Appendix for visualizations).

6.3 Extension to Lorentz Group

To examine our method’s generalization capability, we apply it to top quark tagging, a classification task with Lorentz symmetry ($O(1, 3)$), noting that $SO(3)$ is a subgroup of $O(1, 3)$. Given that inputs lie in \mathbb{R}^4 , we model symmetry discovery within $\bigoplus SO(4)$. Our method achieves an accuracy of 88.03%, which is competitive with approaches explicitly incorporating complete Lorentz symmetry (89.96%). The learned rotation rates $\lambda = [1, 0.00008]$ closely approximate the ground truth $[1, 0]$, with a cosine distance of 3×10^{-6} , demonstrating strong alignment. These results underscore the broader applicability and robust interpretability of our framework beyond $SO(n)$.

Table 6.2: Comparison of symmetry discovery methods. Our method is limited to one-parameter subgroups of $SO(n)$, but combines symmetry discovery, inductive bias, and equivariant prediction in a unified (end-to-end) and interpretable framework. “ \pm ” indicates averaging predictions over multiple transformed inputs at test time.

Aspect	H_γ^{inv} -Net (ours)	LieGG	BNN	LieGAN	Augerino
Equivariant/Invariant Model	✓	✗	✓	✗	✗
Inductive Bias	Strong	None	Strong	None	Weak
Interpretability	High	Low	Moderate	Low	Low
Unified Framework	✓	✗	✓	✗	±
Test-Time Strategy	Direct	Direct	Direct	Direct	Sampling
Symmetry Scope	1D subgroups of $SO(n)$	General	Compact	General	General

7 Conclusion

We proposed a framework for automatic discovery of one-parameter subgroups of $SO(n)$ and their application to learning H_γ -invariant functions. Our method jointly learns the symmetry parameters and the target function in an end-to-end fashion, yielding interpretable and structured models. It consistently outperforms existing symmetry discovery methods such as LieGAN and Augerino across

a range of tasks. On both synthetic and real-world problems—including quantum systems, double pendulum modeling, moment of inertia prediction, and top quark tagging—our approach successfully recovers the rotation rates λ and achieves cosine distances near zero, indicating strong alignment with ground truth symmetries.

This work focuses on one-parameter subgroups of $SO(n)$ under the standard action on \mathbb{R}^n . Extending the framework to operate on higher-order tensors (e.g., matrices) and to discover one-parameter subgroups in broader Lie groups, such as the Lorentz group, represents an important direction for future research.

References

- [1] Taco Cohen and Max Welling. Group equivariant convolutional networks. *International conference on machine learning*, pages 2990–2999, 2016.
- [2] Daniel E Worrall, Stephan J Garbin, Daniyar Turmukhambetov, and Gabriel J Brostow. Harmonic networks: Deep translation and rotation equivariance. *Proceedings of the IEEE conference on computer vision and pattern recognition*, pages 5028–5037, 2017.
- [3] Nathaniel Thomas, Tess Smidt, Steven Kearnes, Lusann Yang, Li Li, Kai Kohlhoff, and Patrick Riley. Tensor field networks: Rotation-and translation-equivariant neural networks for 3d point clouds. *arXiv preprint arXiv:1802.08219*, 2018.
- [4] Fabian B Fuchs, Daniel E Worrall, Volker Fischer, and Max Welling. $Se(3)$ -transformers: 3d roto-translation equivariant attention networks. *Advances in Neural Information Processing Systems*, 2020.
- [5] Maurice Weiler, Fred A Hamprecht, and Martin Storath. 3d steerable cnns: Learning rotationally equivariant features in volumetric data. *Advances in Neural Information Processing Systems*, 2018.
- [6] Manzil Zaheer, Satwik Kottur, Siamak Ravanbakhsh, Barnabas Poczos, Ruslan Salakhutdinov, and Alexander Smola. Deep sets. *Advances in neural information processing systems*, 30, 2017.
- [7] Maurice Weiler and Giacomo Cesa. General $e(2)$ -equivariant steerable cnns. *Advances in Neural Information Processing Systems*, 32, 2019.
- [8] Brian Hall. *Lie groups, Lie algebras, and representations: An elementary introduction*, volume 222. Springer, 2015.
- [9] Anthony W Knapp. *Lie groups beyond an introduction*, volume 140. Springer Science & Business Media, 2002.
- [10] John Stillwell. *Naive Lie theory*. Springer Science & Business Media, 2008.
- [11] Richard M Murray, Zexiang Li, and S Shankar Sastry. *A mathematical introduction to robotic manipulation*. CRC press, 1994.
- [12] William Fulton and Joe Harris. *Representation theory: A first course*, volume 129. Springer Science & Business Media, 1991.
- [13] Marc Finzi, Max Welling, and Andrew Gordon Wilson. A practical method for constructing equivariant multilayer perceptrons for arbitrary matrix groups. In *International conference on machine learning*, pages 3318–3328. PMLR, 2021.
- [14] Michael M Bronstein, Joan Bruna, Yann LeCun, Arthur Szlam, and Pierre Vandergheynst. Geometric deep learning: going beyond euclidean data. *IEEE Signal Processing Magazine*, 34(4):18–42, 2017.
- [15] Michael M Bronstein, Joan Bruna, Taco Cohen, and Petar Veličković. Geometric deep learning: Grids, groups, graphs, geodesics, and gauges. *arXiv preprint arXiv:2104.13478*, 2021.
- [16] Risi Kondor and Shubhendu Trivedi. On the generalization of equivariance and convolution in neural networks to the action of compact groups. In *International conference on machine learning*, pages 2747–2755. PMLR, 2018.
- [17] Taco S Cohen, Mario Geiger, and Maurice Weiler. A general theory of equivariant cnns on homogeneous spaces. *Advances in neural information processing systems*, 32, 2019.
- [18] Patrice Y Simard, David Steinkraus, and John C Platt. Best practices for convolutional neural networks applied to visual document analysis. *Icdar*, 3:958–962, 2003.
- [19] Alex Krizhevsky, Ilya Sutskever, and Geoffrey E Hinton. Imagenet classification with deep convolutional neural networks. pages 1097–1105, 2012.
- [20] Luis Perez and Jason Wang. The effectiveness of data augmentation in image classification using deep learning. *arXiv preprint arXiv:1712.04621*, 2017.
- [21] Víctor Garcia Satorras, Emiel Hoogeboom, and Max Welling. $E(n)$ equivariant graph neural networks. In *International conference on machine learning*, pages 9323–9332. PMLR, 2021.
- [22] Maurice Weiler, Fred A Hamprecht, and Martin Storath. Learning steerable filters for rotation equivariant cnns. In *Proceedings of the IEEE Conference on Computer Vision and Pattern Recognition*, pages 849–858, 2018.

- [23] Maurice Weiler and Gabriele Cesa. General $\mathbf{e}(2)$ -equivariant steerable cnns. *Advances in neural information processing systems*, 32, 2019.
- [24] David Ruhe, Jayesh K Gupta, Steven De Keninck, Max Welling, and Johannes Brandstetter. Geometric clifford algebra networks. In *International Conference on Machine Learning*, pages 29306–29337. PMLR, 2023.
- [25] Sourya Basu, Suhas Lohit, and Matthew Brand. G-repsnet: A fast and general construction of equivariant networks for arbitrary matrix groups. *arXiv preprint arXiv:2402.15413*, 2024.
- [26] Artem Moskalev, Anna Sepliarskaia, Ivan Sosnovik, and Arnold Smeulders. Liegg: Studying learned lie group generators. *Advances in Neural Information Processing Systems*, 35:25212–25223, 2022.
- [27] Marc Finzi, Samuel Stanton, Pavel Izmailov, and Andrew Gordon Wilson. Generalizing convolutional neural networks for equivariance to lie groups on arbitrary continuous data. In *International Conference on Machine Learning*, pages 3165–3176. PMLR, 2020.
- [28] Risi Kondor, Zhen Lin, and Shubhendu Trivedi. Clebsch–gordan nets: a fully fourier space spherical convolutional neural network. *Advances in Neural Information Processing Systems*, 31, 2018.
- [29] Nima Dehmamy, Robin Walters, Yanchen Liu, Dashun Wang, and Rose Yu. Automatic symmetry discovery with lie algebra convolutional network. *Advances in Neural Information Processing Systems*, 34:2503–2515, 2021.
- [30] Nate Gruver, Marc Finzi, Micah Goldblum, and Andrew Gordon Wilson. The lie derivative for measuring learned equivariance. *arXiv preprint arXiv:2210.02984*, 2022.
- [31] Jianke Yang, Robin Walters, Nima Dehmamy, and Rose Yu. Generative adversarial symmetry discovery. In *Proceedings of the 40th International Conference on Machine Learning (ICML)*, 2023. URL <https://arxiv.org/abs/2302.00236>.
- [32] Gregory Benton, Marc Finzi, Pavel Izmailov, and Andrew Gordon Wilson. Learning invariances in neural networks. In *Advances in Neural Information Processing Systems (NeurIPS)*, volume 33, pages 17605–17616, 2020. URL <https://arxiv.org/abs/2010.11882>.
- [33] Sophia Sanborn, Christian Shewmake, Bruno Olshausen, and Christopher Hillar. Bispectral neural networks. *arXiv preprint arXiv:2209.03416*, 2022. URL <https://arxiv.org/abs/2209.03416>.
- [34] Kaiming He, Xiangyu Zhang, Shaoqing Ren, and Jian Sun. Deep residual learning for image recognition. 10.48550. *arXiv preprint arXiv:1512.03385*, 2015.

A Proofs and additional theoretical results

Theorem 4.2 (One-parameter subgroups of $SO(3)$). *Any H_γ -invariant function of the form $\Psi : X \subseteq \mathbb{R}^3 \rightarrow \mathbb{R}^m$ can be expressed as:*

$$\Psi(x) = \phi \left((a_1^T x)^2 + (a_2^T x)^2, a_3^T x \right), \quad (2)$$

for some $\phi : \mathbb{R}^2 \rightarrow \mathbb{R}^m$, where $\{a_i^T\}$ are rows of some $A \in SO(3)$.

Proof. As discussed in Remark 4.1, every one-parameter subgroup of $SO(3)$ is isomorphic to $SO(2)$. Thus, H_γ -invariance corresponds to $SO(2)$ -invariance in an appropriate plane, whose orientation in \mathbb{R}^3 is defined by a suitable $A \in SO(3)$. The $SO(2)$ -invariance preserves the norm of 2-dimensional vectors, leading to diffeomorphism between the quotient space $\mathbb{R}^2/SO(2)$ and $\mathbb{R}_{\geq 0}$. Consequently, for a fixed value of $a_3^T x = c$, the orbits under the action of H_γ correspond one-to-one with the unique norm values of the 2-dimensional vectors $[a_1^T x, a_2^T x]^T$. Formally, the following sets have the same cardinality:

$$\begin{aligned} S_1 &= \{\mathcal{O}(x; H_\gamma) : x \in X, a_3^T x = c\}, \\ S_2 &= \left\{ (a_1^T x)^2 + (a_2^T x)^2 : x \in X \right\}. \end{aligned}$$

Since learning an H_γ -invariant function corresponds to learning appropriate values for these orbits, the invariant function takes the standard form given in equation 2. \square

Proposition 4.4 (Orbit Representation). *Let H_γ be a one-parameter subgroup of $SO(n)$ defined by $A \in SO(n)$ and rotation rates $\{\lambda_i\}$. For any $x \in \mathbb{R}^n$, its orbit under the action of H_γ is*

$$\mathcal{O}_{H_\gamma}(x) = \mathcal{O}_{H_\gamma}(A^T \text{invRep}(x)).$$

Proof. We just have to show that,

$$A^T \text{invRep}(x) = A^T \left(\|v_1\| e_1 \bigoplus_{i=2}^{\frac{n}{2}} R(-t_0 \lambda_i) v_i \right) \in \mathcal{O}_{H_\gamma}(x)$$

That is, for some t'

$$\begin{aligned} A^T \left(\|v_1\| e_1 \bigoplus_{i=2}^{\frac{n}{2}} R(-t_0 \lambda_i) v_i \right) &= A^T \left(\bigoplus_{i=1}^{\frac{n}{2}} R(-t' \lambda_i) \right) Ax \\ &= A^T \left(\bigoplus_{i=1}^{\frac{n}{2}} R(-t' \lambda_i) \right) \bigoplus_{i=1}^{\frac{n}{2}} v_i \\ &= A^T \left(\bigoplus_{i=1}^{\frac{n}{2}} R(-t' \lambda_i) v_i \right) \end{aligned}$$

Choose $t' = t_0$, we get,

$$\begin{aligned} A^T \left(\bigoplus_{i=1}^{\frac{n}{2}} R(-t' \lambda_i) v_i \right) &= A^T \left(\bigoplus_{i=1}^{\frac{n}{2}} R(-t_0 \lambda_i) v_i \right) \\ &= A^T \left(R(-t_0 \lambda_1) v_1 \bigoplus_{i=2}^{\frac{n}{2}} R(-t_0 \lambda_i) v_i \right) \\ &= A^T \left(\|v_1\| e_1 \bigoplus_{i=2}^{\frac{n}{2}} R(-t_0 \lambda_i) v_i \right) \end{aligned}$$

Hence, $A^T \left(\|v_1\| e_1 \bigoplus_{i=2}^{\frac{n}{2}} R(-t_0 \lambda_i) v_i \right) \in \mathcal{O}_{H_\gamma}(x)$. \square

Proposition 4.5 (Orbit Separation). *The function invRep is in bijective correspondence with the orbits of X under the action of the one-parameter subgroup H_γ . Specifically, for any $x, x' \in \mathbb{R}^n$,*

$$\mathcal{O}_{H_\gamma}(x) = \mathcal{O}_{H_\gamma}(x') \iff \text{invRep}(x) = \text{invRep}(x').$$

Hence, invRep is both invariant under H_γ and separates the orbits of H_γ .

Proof. Suppose $\mathcal{O}_{H_\gamma}(x) = \mathcal{O}_{H_\gamma}(x')$. Then:

$$\begin{aligned} x' &\in \mathcal{O}_{H_\gamma}(x) \\ \implies \exists t' \in \mathbb{R} \text{ such that } A^T \bigoplus_{i=1}^{\frac{n}{2}} R(t' \lambda_i) Ax &= x'. \end{aligned} \tag{7}$$

We have,

$$\text{invRep}(x) = \|v_1\|_2 e_1 \bigoplus_{i=2}^{\frac{n}{2}} R(-t_0 \lambda_i) v_i,$$

where t_0 is chosen such that $R(t_0 \lambda_1) e_1 = \frac{v_1}{\|v_1\|_2}$ and $Ax = v = \bigoplus_{i=1}^{\frac{n}{2}} v_i$.

Now, to compute $\text{invRep}(x')$, consider:

$$\begin{aligned} v' &= Ax' \\ &= \bigoplus_{i=1}^{\frac{n}{2}} R(t' \lambda_i) v_i \quad \text{from equation 7} \\ &= \bigoplus_{i=1}^{\frac{n}{2}} v'_i \end{aligned} \tag{8}$$

where:

$$v'_i = R(t' \lambda_i) v_i, \text{ and note that } \|v'_i\|_2 = \|v_i\|_2.$$

Choose t_1 such that:

$$R(t_1 \lambda_1) e_1 = \frac{v'_1}{\|v'_1\|}.$$

Substitute v'_1 :

$$R(t_1 \lambda_1) e_1 = \frac{R(t' \lambda_1) v_1}{\|v_1\|_2}$$

$$\begin{aligned} R(t_1 \lambda_1) e_1 &= R(t' \lambda_1) \frac{v_1}{\|v_1\|_2} \\ &= R(t' \lambda_1) R(t_0 \lambda_1) e_1 \\ R(t_1 \lambda_1) e_1 &= R((t' + t_0) \lambda_1) e_1 \end{aligned}$$

Thus, by properties of rotation matrices:

$$R(t_1 \lambda_1) = R((t' + t_0) \lambda_1).$$

We can set $t_1 = t' + t_0$.

Finally:

$$\begin{aligned}
\text{invRep}(x') &= \|v'_1\|_2 e_1 \bigoplus_{i=2}^{\frac{n}{2}} R(-t_1 \lambda_i) v'_i \\
&= \|v_1\|_2 e_1 \bigoplus_{i=2}^{\frac{n}{2}} R(-t' \lambda_i - t_0 \lambda_i) R(t' \lambda_i) v_i \\
&= \|v_1\|_2 e_1 \bigoplus_{i=2}^{\frac{n}{2}} R(-t_0 \lambda_i) v_i \\
&= \text{invRep}(x)
\end{aligned}$$

Thus:

$$\mathcal{O}_{H_\gamma}(x) = \mathcal{O}_{H_\gamma}(x') \implies \text{invRep}(x) = \text{invRep}(x').$$

Conversely, suppose $\text{invRep}(x) = \text{invRep}(x')$:

From Proposition 4.4, we have,

$$\begin{aligned}
A^T \text{invRep}(x) &\in \mathcal{O}_{H_\gamma}(x) \\
A^T \text{invRep}(x) &= A^T \text{invRep}(x') \in \mathcal{O}_{H_\gamma}(x')
\end{aligned}$$

Thus:

$$\mathcal{O}_{H_\gamma}(x) \cap \mathcal{O}_{H_\gamma}(x') \neq \emptyset.$$

Since orbits partition X , we get:

$$\mathcal{O}_{H_\gamma}(x) = \mathcal{O}_{H_\gamma}(x').$$

This completes the proof. \square

Theorem 4.6 (One-parameter subgroups of $SO(n)$). *Any H_γ -invariant function of the form $\Psi : X \subseteq \mathbb{R}^n \rightarrow \mathbb{R}^m$ can be expressed as*

$$\Psi(x) = \phi \left(\text{invRep} \left(x; A, \{\lambda_i\}_{i \in [n/2]} \right) \right), \quad (6)$$

for some function $\phi : \mathbb{R}^n \rightarrow \mathbb{R}^m$, where $A \in SO(n)$ and $\{\lambda_i\}$ are the rotation rates.

Proof. From Proposition 4.5, we observe that each orbit under the action of H_γ corresponds to a unique value of $\text{invRep} \left(x; A, \{\lambda_i\}_{i \in [\frac{n}{2}]} \right)$, and vice versa. Since any H_γ -invariant function is essentially defined by its values on the orbits, it follows that the H_γ -invariant function has the form given in equation 6. \square

A.1 Extension to Equivariant Functions

The extension of the canonical form for invariance, as given in equation 6, to the equivariant setting is straightforward. It is defined as:

$$\Psi(x) = R(t_0 \lambda_1) \phi \left(\text{invRep} \left(x; A, \{\lambda_i\}_{i \in [n/2]} \right) \right), \quad (9)$$

where t_0 is chosen as in Definition 4.3.

B Experimental Setup and Implementation Details

This section outlines the architecture, training procedures, and implementation choices used in all experiments across synthetic and real-world tasks.

Function Definitions and Baselines : Table B.1 defines the H_γ -invariant polynomial functions used throughout our evaluation. We additionally introduce polynomial $u(x)$ (omitted from the main paper) to provide comprehensive assessment of invariance properties. We benchmark our method against established approaches including LieGAN [31], Augerino [32], and LieGG [26]; detailed comparisons with LieGG are provided in Section B.2.

Table B.1: H_γ -invariant functions used in synthetic and real-world tasks. The vectors $\{a_i^\top\}$ correspond to the rows of the ground-truth rotation matrix A_0 for the $p(x)$ task. For the functions $q(x)$, $r(x)$, and $u(x)$, the vector v satisfies $\bigoplus_i v_i = A_0 x$, where \bigoplus denotes block-wise decomposition of the rotated input. a_i s and b_i s are scalars and p_i s are matrix polynomials. The invariance properties of $q(x)$ and $r(x)$ are not obvious and are analyzed in Section B.3.

	Equation
$p(x)$	$\sin \left((a_1^\top x)^2 + (a_2^\top x)^2 \right) + (\cos (a_3^\top x))^2$
$q(x)$	$w^T \text{vec} \left(\sum_{i=1}^2 a_i p_i (v_i v_i^\top) \right)$
$r(x)$	$w^T \text{vec} \left(\sum_{i=1}^4 b_i p_i (v_i v_i^\top) \right)$
$u(x)$	$[\ v_i\ _2]_{i=1}^2$
Anisotropic Quantum	$\sum_{i=1}^{n/2} w_i ((A_0 x)_{2i-1}^2 + (A_0 x)_{2i}^2)$
Moment of Inertia	$\sum_{i=1}^N m_i (x_i^\top x_i I - x_i x_i^\top)$

The double pendulum task involves predicting the spring force $\pm k(q_1 - q_2)$, where q_1 and q_2 denote the angles made by the two pendulums with respect to the z -axis. Specifically, given the position vectors x_1, x_2 and the corresponding momenta p_1, p_2 , the goal is to predict the time derivatives $\dot{q}_1, \dot{q}_2, \dot{p}_1, \dot{p}_2$, which are given by $\dot{q}_1 = p_1$, $\dot{q}_2 = p_2$, $\dot{p}_1 = k(q_1 - q_2)$, and $\dot{p}_2 = -k(q_1 - q_2)$.

This system exhibits symmetry under simultaneous rotation of both pendulums by the same angle around the z -axis. That is, rotating the two pendulums equally about the z -axis does not alter the predicted derivatives, indicating invariance to a one-parameter subgroup of the form $SO(2) \oplus SO(2)$. The rotation rates corresponding to this subgroup are $\lambda = [1, 1, 0]$, where the two ones reflect invariance under rotations (simultaneous and same) of the pendulum angles, and the zero indicates no invariance with respect to the magnitudes of the momentum variables.

Training Configuration and Results : Table B.2 presents the mean and standard deviation of both the invariance error and the validation loss (MSE) for the regression tasks involving H_γ -invariant polynomial functions. The cosine distance results, which are applicable only to H_γ^{inv} -Net due to its interpretable symmetry parameters, are reported separately in Table B.3. Each method was evaluated across three independent random seeds. All models underwent training for 100 epochs using the Adam optimizer with learning rate 1e-3. For our experiments, we used an NVIDIA RTX A6000 GPU.

Table B.2: Comparison of H_γ^{inv} -Net (ours), LieGAN [31], and Augerino [32] on H_γ -invariant polynomial tasks. For each method, we report the mean \pm standard deviation of the relevant evaluation metric across multiple runs. A dash (–) indicates that the metric is not applicable to the corresponding method.

Task	Method	Invariance Error	Val. Loss (MSE)
$p(x)$ $n = 3$	H_γ^{inv} -Net	$(1.98 \pm 5.59) \times 10^{-5}$	$(2.46 \pm 0.80) \times 10^{-6}$
	LieGAN	$(8.21 \pm 0.08) \times 10^{-4}$	–
	Augerino	$(1.27 \pm 0.00) \times 10^{-3}$	$(1.22 \pm 0.10) \times 10^{-2}$
$q(x)$ $n = 8$	H_γ^{inv} -Net	$(3.00 \pm 1.00) \times 10^{-4}$	$(5.94 \pm 4.36) \times 10^{-2}$
	LieGAN	$(5.63 \pm 4.98) \times 10^{-2}$	–
	Augerino	$(2.12 \pm 3.13) \times 10^{-2}$	$(1.20 \pm 0.55) \times 10^{-1}$
$r(x)$ $n = 8$	H_γ^{inv} -Net	$(5.83 \pm 7.52) \times 10^{-2}$	$(4.78 \pm 1.49) \times 10^{-1}$
	LieGAN	$(4.89 \pm 3.98) \times 10^1$	–
	Augerino	$(0.217 \pm 0.25) \times 10^1$	$(0.19 \pm 0.10) \times 10^1$

Architecture Specifications : Our neural network $\phi(x)$ employs a 4-layer fully connected architecture featuring ReLU activations in hidden layers and a linear output layer. For Lorentz group experiments,

we substitute ResNet [34] architectures to better capture geometric structure. Baseline methods retain their original configurations as reported in respective publications.

Table B.3: Cosine distances (mean \pm standard deviation) between learned and reference generators for H_γ^{inv} -Net.

Task	Cosine Distance
$p(x)$ ($n = 3$)	$(1.62 \pm 0.54) \times 10^{-2}$
$q(x)$ ($n = 4$)	$(4.03 \pm 1.97) \times 10^{-6}$
$r(x)$ ($n = 8$)	$(6.63 \pm 0.11) \times 10^{-3}$

B.1 Robustness of H_γ^{inv} -Net to Label Noise

Table B.4 reports the robustness of H_γ^{inv} -Net under output perturbations (label noise). We evaluate performance on the functions $u(x)$ and $r(x)$ by adding Gaussian noise with standard deviations 0.001, 0.01, and 0.1. For each noise level, we measure validation loss (MSE) and cosine distance. The results show that H_γ^{inv} -Net maintains strong performance even under substantial noise, indicating robustness and effective generalization.

Table B.4: Results for H_γ^{inv} -Net trained on inputs corrupted with Gaussian noise of varying standard deviations, evaluated on the $u(x)$ and $r(x)$ tasks. We report both the validation error and cosine distance to assess performance under noise.

	Val. Loss (MSE)	Cosine Distance
$u(x)$ ($\sigma = 0.001$)	1.03×10^{-6}	1.00×10^{-7}
$u(x)$ ($\sigma = 0.01$)	3.08×10^{-5}	1.96×10^{-6}
$u(x)$ ($\sigma = 0.1$)	1.90×10^{-3}	1.13×10^{-5}
$r(x)$ ($\sigma = 0.001$)	1.80×10^{-6}	7.00×10^{-5}
$r(x)$ ($\sigma = 0.01$)	1.60×10^{-6}	2.00×10^{-5}
$r(x)$ ($\sigma = 0.1$)	1.60×10^{-6}	1.00×10^{-6}

B.2 Comparison with LieGG

We compare the performance of H_γ^{inv} -Net and LieGG [26] on three tasks: $q(x)$, $r(x)$, and the Double Pendulum system. The results are summarized in Table B.5. For $q(x)$ and $r(x)$, we experiment with different choices of A_0 , and report the mean and standard deviation across these settings. Invariance error measures how well the discovered subgroup captures the symmetry of the function, while validation loss assesses function learning accuracy.

Across all tasks, H_γ^{inv} -Net achieves substantially lower invariance error and validation loss, indicating more accurate symmetry discovery and function learning. The improvement is especially notable for the high-dimensional task $r(x)$. On the Double Pendulum task, LieGG achieves a low validation loss, but its high invariance error suggests poor symmetry alignment. In contrast, H_γ^{inv} -Net performs well and outperforms LieGG on both metrics. Unlike H_γ^{inv} -Net, LieGG does not incorporate a learnable inductive bias and only identifies symmetries post hoc, without enforcing them during training. As a result, the resulting model is not guaranteed to be invariant and lacks interpretability. These findings underscore the end-to-end advantage of H_γ^{inv} -Net over LieGG.

B.3 H_γ -Invariance of q and r

The polynomials q and r defined in Table B.1 are similar with different input dimension. We will demonstrate the invariance property for generic n (even n), the corresponding polynomial is denoted by ρ . The polynomial ρ is defined as:

Table B.5: Comparison of H_γ^{inv} -Net and LieGG on $q(x)$, $r(x)$, and Double Pendulum tasks. Mean \pm std is reported for $q(x)$ and $r(x)$; single-run results are shown for Double Pendulum. Best values per task are highlighted in .

Task	Method	Invariance Error	Val. Loss (MSE)
$q(x)$ ($n = 4$)	H_γ^{inv} -Net	$(3.00 \pm 1.00) \times 10^{-4}$	$(5.94 \pm 4.36) \times 10^{-2}$
	LieGG	(7.90 ± 5.32)	(0.276 ± 0.073)
$r(x)$ ($n = 8$)	H_γ^{inv} -Net	$(5.83 \pm 7.52) \times 10^{-2}$	$(4.78 \pm 1.49) \times 10^{-1}$
	LieGG	(98.62 ± 85.86)	(1.943 ± 1.284)
Double Pendulum ($n = 8$)	H_γ^{inv} -Net	0.17	5.59×10^{-6}
	LieGG	2.028	2.33×10^{-5}

$$\rho(x) = w^T \text{vec} \left(\sum_{i=1}^{n/2} p_i(v_i v_i^T) \right) = \rho^{(\text{inv})} \circ \rho^{(\text{equi})}$$

where

$$\rho^{(\text{inv})}(W) = w^T \text{vec}(W), \quad \rho^{(\text{equi})}(x) = \sum_{i=1}^{n/2} p_i(v_i v_i^T),$$

with

$$v = \bigoplus_{i=1}^4 v_i = A_0 x,$$

and $\{p_i\}$ being polynomials in matrices.

Since $\{p_i\}$ are polynomials in matrices, ρ satisfies the following transformation property:

$$\rho^{(\text{equi})} \left(A_0^T \bigoplus_{i=1}^4 R(t) A_0 x \right) = R(t) \rho^{(\text{equi})}(x) R(t)^T \quad (10)$$

Furthermore, selecting w from the following subspace that satisfies the equivariance constraints (as derived in Section 4 of EMLP [13]):

$$w \in \text{span} \left\{ \begin{bmatrix} 1 \\ 0 \\ 0 \\ 1 \end{bmatrix}, \begin{bmatrix} 0 \\ 1 \\ -1 \\ 0 \end{bmatrix} \right\}. \quad (11)$$

ensures that,

$$\rho^{(\text{inv})} \left(R(t) \rho^{(\text{equi})}(x) R(t)^T \right) = \rho^{(\text{inv})} \left(\rho^{(\text{equi})}(x) \right), \quad (12)$$

Applying equation 10 and equation 12, we derive the overall invariance condition:

$$\rho \left(A^T \bigoplus_{i=1}^{n/2} R(t) A x \right) = \rho(x). \quad (13)$$

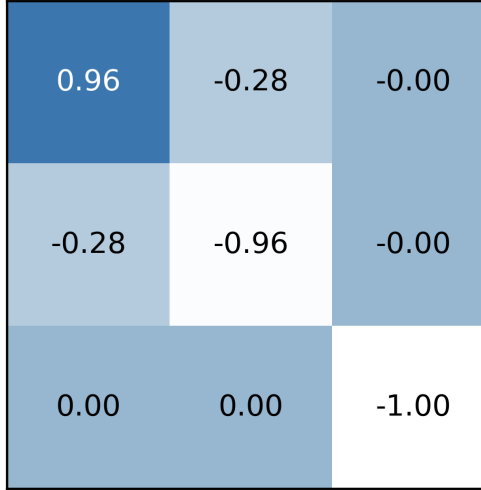
This result confirms that ρ remains invariant under the given transformations, establishing its suitability for learning tasks that require H_γ -invariance in $SO(n)$.

B.4 Code

Our implementation is available at https://anonymous.4open.science/r/Automatic_discovery_so_n-7664/

B.5 Interpretability

As discussed in Section 6.2 of the main paper, the theoretical result regarding the interpretability of the learnt A concerning the reference A_0 is as follows:



(a) $p(x)$

Figure 4: Matrix representation of $A_0^T A$ for the $p(x)$ task with dimension $n = 3$, trained using H_{inv}^γ -Net, where A_0 denotes the ground-truth rotation matrix and A is the learned rotation matrix. The matrix product highlights the alignment between the learned and true symmetry transformations.

Proposition B.1 (Interpretability). *Let n be even and set $M = n/2$. Write any $A \in \text{SO}(n)$ as an $M \times M$ block matrix $A = [R_{ij}]_{i,j=1}^M$ with $R_{ij} \in \mathbb{R}^{2 \times 2}$, and factor A as $A = A_1^\top A_2$ with $A_1, A_2 \in \text{SO}(n)$.*

Define the one-parameter subgroups

$$H_1 = \left\{ A_1 \bigoplus_{i=1}^M R(\theta) A_1^\top : \theta \in [0, 2\pi] \right\}, \quad H_2 = \left\{ A_2 \bigoplus_{i=1}^M R(\theta) A_2^\top : \theta \in [0, 2\pi] \right\},$$

where $R(\theta) \in \text{SO}(2)$ is a planar rotation. If, for every $\theta \in [0, 2\pi]$,

$$\sum_{j=1}^M R_{ji}^\top R(\theta) R_{jk} = O_2 \quad (2 \times 2 \text{ zero matrix}), \quad i \neq k, \quad (14)$$

$$\sum_{j=1}^M R_{ji}^\top R(\theta) R_{ji} = R(\theta), \quad i = 1, \dots, M, \quad (15)$$

then $H_1 = H_2$; that is, A_1 and A_2 generate the same one-parameter subgroup.

Proof. Consider $A^\top \left(\bigoplus_{i=1}^M R(\theta) \right) A$ represented as an $M \times M$ block matrix, where each block is 2×2 . Then, each such block is given by:

$$\left[A^\top \left(\bigoplus_{i=1}^M R(\theta) \right) A \right]_{ik} = \begin{cases} \sum_{j=1}^M R_{ji}^\top R(\theta) R_{jk}, & i \neq k, \\ \sum_{j=1}^M R_{ji}^\top R(\theta) R_{ji}, & \text{otherwise} \end{cases}; \quad \forall i, k \in \{1, 2, \dots, M\} \quad (16)$$

Conditions given in equation 14–equation 15 imply,

$$A^\top \left(\bigoplus_{i=1}^M R(\theta) \right) A = \bigoplus_{i=1}^M R(\theta). \quad (17)$$

Substituting $A = A_1^\top A_2$ gives

$$A_2^\top A_1 \left(\bigoplus_{i=1}^M R(\theta) \right) A_1^\top A_2 = \bigoplus_{i=1}^M R(\theta). \quad (18)$$

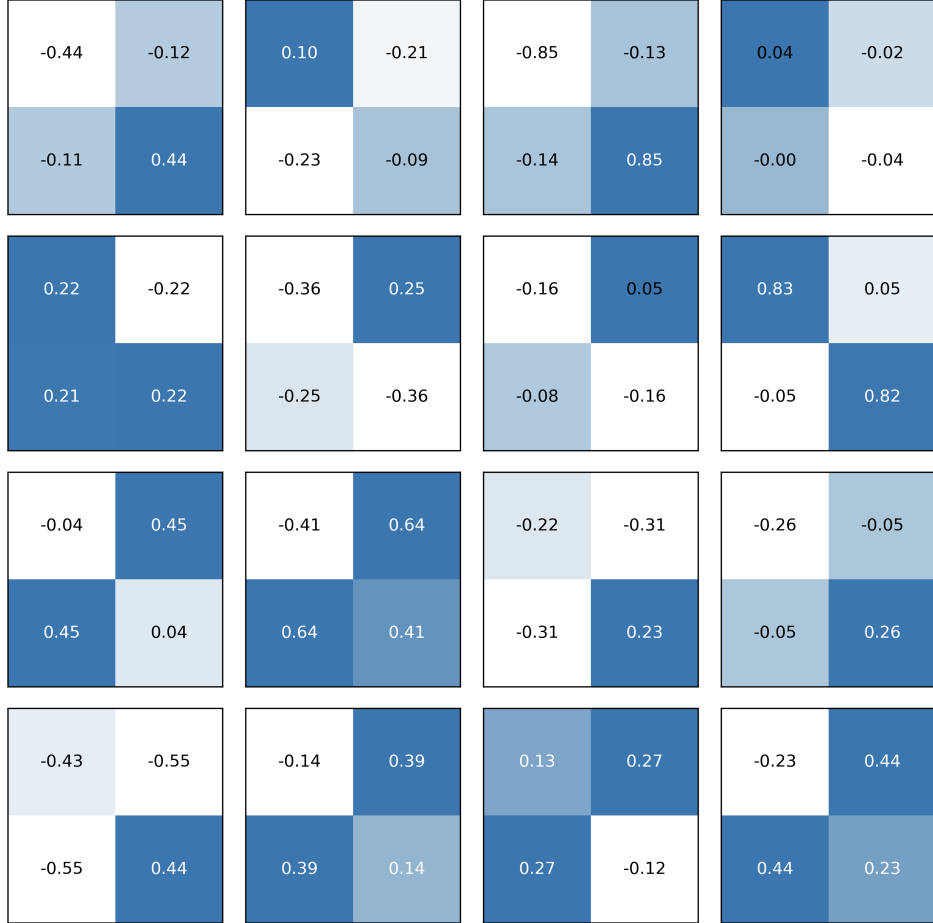
Multiplying on the left by A_2 and on the right by A_2^\top yields

$$A_1 \left(\bigoplus_{i=1}^M R(\theta) \right) A_1^\top = A_2 \left(\bigoplus_{i=1}^M R(\theta) \right) A_2^\top, \quad (19)$$

so the two subgroups coincide, $H_1 = H_2$. \square

Remark B.2. If the function remains invariant under a rotation $R(-\theta)$ instead of $R(\theta)$ in some of the 2D planes, then multiple valid one-parameter subgroups exist. In such cases, the condition in equation 15 must be modified by replacing $R(\theta)$ with $R(-\theta)$ on the right-hand side for the corresponding block indices i .

The above result can be applied to our experiments by identifying $A_1 = A_0$ (the reference matrix) and $A_2 = A$ (the learned matrix), allowing us to verify whether they correspond to the same one-parameter subgroup. We visualize the matrix product $A_0^\top A$ for the regression tasks involving the polynomials $p(x)$ and $r(x)$ (defined in Table B.1) in Figure 4 and Figure 5, respectively. We have further verified empirically that the conditions in equation 15 and equation 14 hold across all experimental cases considered.



(a) $r(x)$

Figure 5: Matrix representation of $A_0^T A$ for the $r(x)$ task with dimension $n = 8$, trained using H_{inv}^γ -Net. Analysis shows that ground rotation matrix A_0 and the learnt rotation matrix A have different numerical values, but they capture the one-parameter subgroups for the given functions. This relationship is confirmed by the structure of $A_0^T A$, which takes the form consisting of 2×2 blocks of scaled orthonormal matrices. The presence of this structure verifies that the learnt representation effectively captures the underlying symmetry properties, despite differences in specific numerical values.

NeurIPS Paper Checklist

1. Claims

Question: Do the main claims made in the abstract and introduction accurately reflect the paper's contributions and scope?

Answer: [\[Yes\]](#)

Justification: The abstract and introduction clearly state the contributions, including the discovery of one-parameter subgroups and learning invariant functions, which are demonstrated through theory and experiments.

2. Limitations

Question: Does the paper discuss the limitations of the work performed by the authors?

Answer: [\[Yes\]](#)

Justification: Limitations are discussed in Section 7, including the restriction to one-parameter subgroups of $SO(n)$.

3. Theory assumptions and proofs

Question: For each theoretical result, does the paper provide the full set of assumptions and a complete (and correct) proof?

Answer: [\[Yes\]](#)

Justification: Theorems and propositions are formally stated in main paper and proved in the Appendix.

4. Experimental result reproducibility

Question: Does the paper fully disclose all the information needed to reproduce the main experimental results?

Answer: [\[Yes\]](#)

Justification: Experimental settings, architectures, and evaluation metrics are detailed in Section 5 and Appendix.

5. Open access to data and code

Question: Does the paper provide open access to the data and code?

Answer: [\[Yes\]](#)

Justification: A zip file containing the code is provided in the supplementary material.

6. Experimental setting/details

Question: Does the paper specify all training and test details?

Answer: [\[Yes\]](#)

Justification: See Section 5 and Appendix for full training and evaluation details.

7. Experiment statistical significance

Question: Does the paper report error bars or other statistical significance info?

Answer: [\[Yes\]](#)

Justification: We report validation error and cosine distance across multiple runs. For selected tasks, error bars are reported in the main paper; additional statistical significance results are provided in the Appendix.

8. Experiments compute resources

Question: Does the paper report compute requirements?

Answer: [\[Yes\]](#)

Justification: Appendix lists GPU type, runtime, and total compute hours.

9. Code of ethics

Question: Does the research conform with the NeurIPS Code of Ethics?

Answer: [\[Yes\]](#)

Justification: The work adheres to the Code of Ethics; it uses synthetic and publicly available data without privacy concerns.

10. Broader impacts

Question: Does the paper discuss potential societal impacts?

Answer: [NA]

Justification: The paper is foundational research in symmetry-aware learning.

11. Safeguards

Question: Are safeguards in place for data/models with high risk of misuse?

Answer: [NA]

Justification: No such models or datasets are released or involved.

12. Licenses for existing assets

Question: Are existing assets credited with license info?

Answer: [Yes]

Justification: All datasets and code used from prior work are cited and their licenses are noted in Appendix.

13. New assets

Question: Are new assets well documented?

Answer: [Yes]

Justification: New datasets and code are documented and provided with instructions in the supplementary material.

14. Crowdsourcing and research with human subjects

Question: Does the paper involve human subjects or crowdsourcing?

Answer: [NA]

Justification: No such data or procedures were used.

15. Institutional review board (IRB) approvals or equivalent

Question: Were IRB approvals needed or obtained?

Answer: [NA]

Justification: No human subjects were involved in the research.

16. Declaration of LLM usage

Question: Does the paper use LLMs in a non-standard way that affects core methodology?

Answer: [NA]

Justification: LLMs were not used in the development of the core methods.